AIAA SciTech Forum
12-16 January 2026, Orlando, FL
AIAA SCITECH 2026 Forum

10.2514/6.2026-0860

Atmospheric Turbulence Modelling for Very Large Wind Turbines

N.S. Dangi*, J. Sodja †, D.A. von Terzi ‡ and W. Yu §
Delft University of Technology (TU Delft), Aerospace Engineering, 2629 HS, Delft, Netherlands

Accurate modeling of atmospheric turbulence is critical for the design and operation of next-generation large-scale wind turbines, particularly those exceeding 15 MW rated capacity and spanning well above the atmospheric surface layer (typically 10 – 20% of the atmospheric boundary layer (ABL)). In this study, Large Eddy Simulations (LES) were performed to investigate turbulence characteristics at high altitudes, up to 300 m above ground level — a region increasingly relevant for large turbine rotors. Turbulence coherence was analyzed and compared with field measurements to assess the fidelity of numerical predictions. Coherence estimates from LES were validated against lidar-based measurements obtained under stable, neutral, and unstable atmospheric conditions. Results show good agreement in the coherence decay rates and cross-spectral characteristics, with notable discrepancies only at very low frequencies (on the order of several 10^{-4} Hz) and large spatial separations (on the order of several 10^{2} m). Consequently, a LES-tuned empirical lateral coherence model is proposed, featuring distinct coherence decay rates for each atmospheric stability regime (stable, neutral, and unstable ABL), offering improved representation of turbulence structures across a range of operating conditions. These findings provide a valuable reference for refining turbulence models for improving load estimation methodologies for next-generation wind turbines operating at hub heights above 200 m.

I. Nomenclature

γ^2	=	Magnitude squared coherence (-)
Δy	=	Lateral separation (m)
Δz	=	Vertical separation (m)
a_y	=	Decay parameter for the y direction (-)
β_y	=	Decay exponent for the y direction (-)
f	=	Frequency (Hz)
NABL	=	Neutral atmospheric boundary layer
SABL	=	Stable atmospheric boundary layer
USABL	=	Unstable atmospheric boundary layer

II. Introduction

As wind energy development progresses toward larger, more powerful turbines—exceeding 15 MW rated capacity and reaching rotor heights well above 200 m —the need for accurate characterization of atmospheric turbulence at high altitudes has become increasingly critical [1]. These large wind turbines operate in regions that extend beyond the traditional atmospheric surface layer (typically 10 – 20% of the atmospheric boundary layer (ABL)), where conventional turbulence models, originally developed for lower altitudes and suitable for smaller turbines, may no longer suffice [2, 3].

Turbulence impacts wind turbine performance, structural loading, and control strategies, and thus directly influences the reliability and cost-effectiveness of structures influenced by wind loading [1, 4]. One key aspect of turbulence relevant to wind turbine design is spatial coherence—the degree to which wind fluctuations are correlated across different locations in space [5, 6].

*PhD Researcher, Wind Energy, TU Delft
†Assistant Professor, Aerospace Structures and Materials, TU Delft.
‡Professor, Wind Energy, TU Delft.
§Assistant Professor, Wind Energy, TU Delft.

Despite its importance, the modeling of turbulence coherence at altitudes relevant to modern turbines remains a challenge due to the scarcity of field measurements, specifically at scales relevant for very-large wind turbines and limitations in existing parametric models. For instance, the measurements in [2, 6, 7, 8, 9] are for altitudes lower than 100 m while 20 MW wind turbine can reach altitudes of 300 m [10]. Even though Large Eddy Simulation (LES) has emerged as a powerful tool for resolving turbulence structures in the atmospheric boundary layer (ABL), offering a high-fidelity numerical approach to complement and interpret field observations, a similarly lacking analysis for high altitudes is evident in numerical simulations. The current wind turbine design standard laid out in the International Electrotechnical Commission (IEC) [11] document makes use of two spectral methods for wind field generation, the more physical Mann model [12, 13] and the method hereafter referred to as, the Kaimal model, given by the Kaimal auto spectrum [14] with the modified [15] Davenport's exponential coherence model [16]. However, both models are intended for use in the atmospheric surface layer and not for the intricate atmospheric boundary layer dynamics at higher altitudes. Furthermore the models are intended for use in neutral atmospheric conditions while offshore environments are frequently characterized by non-neutral conditions [2, 17, 18]. More specifically, the coherence function given in the IEC Kaimal model does not model the dependence of coherence decay parameter on separation and does not take into account change in coherence with altitudes; a dependence which was found necessary [19, 20, 21, 22]. Furthermore, it does not distinguish between coherence modelling for the different velocity components [1] and also does not distinguish between coherence for lateral and vertical separations.

This study aims to tackle these limitations and improve the understanding and modeling of atmospheric turbulence coherence at altitudes up to 300 m. LES is employed to generate turbulence under different atmospheric stability regimes, and the results are validated against lidar-based field measurements obtained from the Technical University of Denmark (DTU) [23].

This article focuses on two research questions: (1) How do atmospheric spectral characteristics compare between LES and field measurements? (2) How can the wind field coherence be modelled in a simple yet representative manner? Consequently, the novel aspects of this article are: (1) Measurement validated LES of different atmospheric boundary layers at scales relevant for 20 MW+ wind turbines, (2) Tuned lateral coherence models for the longitudinal and lateral velocity components in different atmospheric stabilities.

III. Methodology

The two main methods used in this study are high-fidelity numerical simulations using LES and low-fidelity numerical simulations using coherence models to simulate a wind field.

A. Large eddy simulations

The widely used open-source high-fidelity tool NREL SOWFA * [24] was utilized to generate LES-based precursor ABL wind fields. NREL SOWFA is a set of computational fluid dynamics (CFD) solvers, boundary conditions, and turbine models. SOWFA simulates the ABL and is coupled to OpenFOAM [25] and NREL OpenFAST [26]. Below is a short description of the LES solver, in line with nomenclature from [27].

The spatially filtered, incompressible Navier–Stokes equations to give the resolved-scale (large-eddy scale) dynamics of fluid flow incorporate the filtered continuity equation $\frac{\partial \bar{u}_j}{\partial x_j} = 0$, where the overbar denotes spatial filtering and $\bar{u}_j = u_j - u_j^{'}$ is the resolved-scale velocity vector, which is the instantaneous velocity vector, u_j, minus the subfilter-scale (SFS) velocity vector, $u_j^{'}$. The filtered momentum equation is shown in Equation 1.

$$\frac{\partial \bar{u}_i}{\partial t} + \frac{\partial}{\partial x_j}\left(\bar{u}_j \bar{u}_i\right) = \underbrace{-2\epsilon_{i3k}\Omega_3 \bar{u}_k}_{\text{I}} - \underbrace{\frac{\partial \tilde{p}}{\partial x_i}}_{\text{II}} \underbrace{-\frac{1}{\rho_0}\frac{\partial}{\partial x_i} p_0(x,y)}_{\text{III}} \underbrace{-\frac{\partial \tau_{ij}^D}{\partial x_j}}_{\text{IV}} \underbrace{+g\left(\frac{\bar{\theta}-\theta_0}{\theta_0}\right)\delta_{i3}}_{\text{V}} + \underbrace{\frac{1}{\rho_0}F_i^T}_{\text{VI}} \tag{1}$$

Term I is the Coriolis force due to planetary rotation, and ϵ_{ijk} is the alternating tensor. The rotation rate vector is given as, $\Omega = \omega[0, \cos(\phi), \sin(\phi)]$, where ω is the planetary rotation rate and ϕ is the latitude. Term II is the gradient of the

*NREL SOWFA-6 was used in this study and is hereafter referred to as NREL SOWFA.

modified pressure variable. Term III represents the background driving pressure gradient. Term IV is the divergence of the deviatoric part of the fluid stress tensor which is composed of a viscous and an SFS part. The one equation eddy-viscosity SFS model from [28, 29] was used. Term V is used to model buoyancy effects using the Boussinesq approximation. Term VI accounts for other density normalized forces, if relevant, for example, the body force field exerted in the case of an actuator line turbine model. The equation for the transport of resolved potential temperature is shown in Equation 2.

$$\frac{\partial \bar{\theta}}{\partial t} + \frac{\partial}{\partial x_j}\left(u_j \bar{\theta}\right) = -\frac{\partial q_j}{\partial x_j} \tag{2}$$

Here q_j represents the flux of temperature by viscous and SFS effects. The several precursor ABLs were generated within an empty domain 4.5 km × 3 km × 1 km. The details about the simulation set-up can be found in [30]. Nevertheless, a short description of the simulation set-up is provided here. The precursors were simulated with offshore conditions by utilizing a surface roughness of 0.0001 m. To achieve a fully developed ABL, the precursors were simulated for 20000 s for cases with neutral ABL (NABL) and unstable ABL (USABL) and 25000 s for cases with stable ABL [31] (SABL). This disparity in duration aimed to accommodate more complex development of shear, leading to low-level jet-like scenarios. The Coriolis parameter was calculated using a latitude of 52.8 deg, representative of the Dutch North Sea [32]. The measurements later shown in this study are for an offshore site at a latitude of 57.5 deg; however, this is not considered to be a significant difference. A capping inversion at 500 m was set for all simulations. The reference potential temperature was set as 300K. Within a 100 m inversion width, the potential temperature was set to vary from 300 K to 305 K. Above the inversion layer, a potential temperature gradient of 0.003 K/m was specified [27]. On the lower boundary, a temperature flux of −0.02 K-m/s in the altitude direction was applied for the USABL simulations, while a temperature flux of 0.02 K-m/s was applied for the SABL simulations ([33]). The reader is referred to Figure 3 of [30] for the resulting precursor ABL characteristics. It can be noted that a total of nine different LES precursors were generated, which correspond to three different wind speed regimes, each in three different atmospheric stabilities.

B. Coherence models

Spatial and temporal scales of motion can be comprehended utilizing space-time correlation and coherence. The former measures the correspondence of fluctuations at two points over time. The latter is a normalized measure of the correlation between two signals at a given frequency. Two coherence functions are detailed to lay the ground for the proposed model in this article. First, the IEC coherence (γ^2_{IEC}) function for an arbitrary separation r is given in Equation 3 [6, 34].

$$\gamma^2_{\text{IEC}}(r, f) = \left(\exp\left(-12\sqrt{\left(\frac{f \cdot r}{V_{\text{hub}}}\right)^2 + \left(\frac{0.12 \cdot r}{L_{c,\text{IEC}}}\right)^2}\right)\right)^2 \tag{3}$$

where f is the frequency in Hz, r represents the length of the projection of the vector that separates the two points onto a plane that is perpendicular to the average direction of the wind, L_c is the coherence scale parameter given as $8.1\Lambda_1$ [34], where $\Lambda_1 = 42$ m is the longitudinal turbulence scale parameter, for wind load analysis of wind turbines with hub heights ≥ 60 m, and V_{hub} is the velocity at the hub height. It can be noted that the IEC coherence function has the following drawbacks— (1) it does not distinguish between lateral and vertical separations given the use of an arbitrary distance r in Equation 3; (2) it does not have a different formulation for different velocity components; (3) it does not distibuish between different atmospheric stabilities; (4) it uses a constant decay parameter and exponent for any separation, 12 and 2, respectively, as seen in Equation 3.

A second coherence function, the Shiotani and Iwatani (1979) coherence function [35] for vertical (z) and lateral (y) directions, hereafter referred to as SHIW model is shown in Equation 4.

$$\begin{aligned} \gamma^2_z &= \exp\left(-a_z f \frac{\Delta z}{V}\right), & \gamma^2_y &= \exp\left(-a_y f \frac{\Delta y}{V}\right), \\ a_z &= 12 + 11\frac{\Delta z}{z}, & a_y &= 28\left(\frac{\Delta y}{z}\right)^{0.45} \end{aligned} \tag{4}$$

From Equation 4, it can be realized that the SHIW coherence model tackles the drawback (1) listed above for the IEC coherence function, partly tackles the drawback (4) in the sense that the decay parameters are a function of separation and altitude but the decay exponent is not present, and lastly it does not tackle the drawback (3). An additional drawback associated with the SHIW coherence model is that it leads to unity coherence at zero frequency. However, [36] state that the coherence does not actually equal unity since the measurement points are separated by a distance that is not small compared to the turbulence length scales.

With the drawbacks of the existing coherence models elaborated, the proposed coherence model is detailed in Equation 6 and Table 2. The comparison of the proposed model with measurements and LES is detailed in section V. Firstly, a mathematical formulation of coherence was employed to estimate the wind field coherence in the measurement-validated LES datasets used in this study for the proposed coherence model. The co-coherence, quad-coherence, and root-coherence were computed (Equation 5, where f is the frequency). These refer to the real part, imaginary part, and amplitude of a two-point cross-spectrum, respectively, normalized by the product of power spectra for each point [36].

$$\gamma = \underbrace{\frac{\mathrm{Re}\left[S_{xy}(f)\right]}{\sqrt{S_{xx}(f)S_{yy}(f)}}}_{\text{co-coherence}} + \underbrace{\frac{\mathrm{Im}\left[S_{xy}(f)\right]}{\sqrt{S_{xx}(f)S_{yy}(f)}}}_{\text{quad-coherence}} \tag{5}$$

The magnitude-squared coherence was then used for modelling purposes of γ^2. All estimates of coherence are provided using the Welch method [37] with seven segments, 50% overlap, and a Hann window function. A simple moving average filter, applied over five points, smoothed the resulting co-coherence estimates. The proposed coherence model is illustrated in Equation 6. To address the drawback (1), two different formulations are employed, inspired by the SHIW coherence function.

$$\boxed{\gamma_z^2 = \exp\left(-a_z\left(\left(f\frac{\Delta z}{V}\right)^{\beta_z} + \left(0.05\frac{\Delta z}{L_{c,IEC}}\right)^{\beta_z}\right)\right), \qquad \gamma_y^2 = \exp\left(-a_y\left(\left(f\frac{\Delta y}{V}\right)^{\beta_y} + \left(0.05\frac{\Delta y}{L_{c,IEC}}\right)^{\beta_y}\right)\right)} \tag{6}$$

However, this article focuses exclusively on lateral coherence. This decision is based on the fact that measurements are only available for lateral separations. As a result, the lateral coherence estimates from the LES data sets could be directly validated against the measurements, whereas such validation was not possible for vertical coherence. Consequently, the authors refrain from modeling vertical coherence in the absence of supporting data. Next, to tackle drawback (2), the proposed model uses different decay parameters (a) and the decay exponent (β) for different velocity components. Thirdly, drawback (3) is tackled by obtaining the fit parameters individually for each atmospheric stability regime. Lastly, drawback (4) is addressed by incorporating the decay exponent (β) into the function. It can also be noted that the non-unity coherence at zero frequency is incorporated by employing the additional term (here, $0.05\Delta_z/L_{c,IEC}$, and $0.05\Delta_y/L_{c,IEC}$) inspired from the IEC coherence function.

The model parameters were obtained by conducting a global optimization of the parameters on the LES datasets. It is worth noting that previous literature aims to provide more physical insights into the model parameters by conducting local optimization and fitting the decay parameter as a function of a physical variable. However, it can be seen that such a method came at the expense of incorrect physical dimensions as seen in the proposed model of [38]. Furthermore, it can also be noted that although the SHIW model provides a fit of the model parameters to separation and altitude (Equation 4), the underlying fit can be seen as non-optimal for most of the data points in their study (Figure 9.4 of [35]).

Hence, here, the model was fit on a subset of the LES coherence dataset using the global optimization approach (as a local optimization was indeed found not to yield a meaningful fit of the decay parameters with a physical variable). Only the coherence estimates at separations of 20 m, 60 m, and 160 m were used, to prevent overfitting, but at all altitudes between 45 m and 300 m in intervals of 20 m were used. The model was then tested against a wider range of separations discussed in section IV.

The global optimization was conducted using the loss function defined in Equation 7, which was applied separately to the different atmospheric stability regimes, the streamwise u component, and the cross-stream v component.

$$\mathcal{L}(a_y, \beta_y) = \sum_{i=1}^{N} w_i \left[\exp\left(-a_y\left(\left(f_i\frac{\Delta y_i}{V_i}\right)^{\beta_y} + \left(0.05\frac{\Delta y_i}{L_{c,IEC}}\right)^{\beta_y}\right)\right) - \gamma_i^{2,\mathrm{obs}}\right]^2 \tag{7}$$

The loss function described in Equation 7 globally minimizes the error between the proposed model and the coherence corresponding to the LES datasets. A simple weighting function $w = 1/(1+f)$ was used to incorporate more weighting to the low-frequency regime. The optimization was conducted using the `MATLAB` function `fmincon`. The model parameters obtained as a result of the global optimization separately for each atmospheric stability regime, wind component, and lateral and vertical separation are provided later in Table 2.

IV. Validation of LES coherence estimations against measurements

The nine distinct LES precursors were post-processed to evaluate the estimates of lateral coherence with the methods described in subsection III.B. The measurement data had a total of 50 different combinations of lateral separation, wind speed conditions, measurement height, and atmospheric stability. The samples that matched the corresponding conditions in the present LES data sets were used for validation; a subset of which is presented here. The measurement-based lateral coherence of the u component ($\gamma^2_{uu,\mathrm{lat}}$) and the v component ($\gamma^2_{vv,\mathrm{lat}}$) is compared with the LES counterpart, and the IEC Kaimal model-based coherence is overlayed to emphasize the motivation behind this study. The measurements [23] were binned for atmospheric stability in accordance with Figure 6 of [2]. The extracted measurements for coherence model development were for the bins of neutral, stable and unstable ABL. The bins were $-0.1 \leq \zeta \leq 0.1$ for NABL, $0.3 < \zeta \leq 1$ for SABL, and $-1 \leq \zeta < -0.3$ for USABL; where $\zeta = z_i/L_{m-o}$ with z_i being the inversion layer height and L_{m-o} the Monin-Obukhov length [39].

First, a comparison for the neutral ABL is provided in Figure 1.

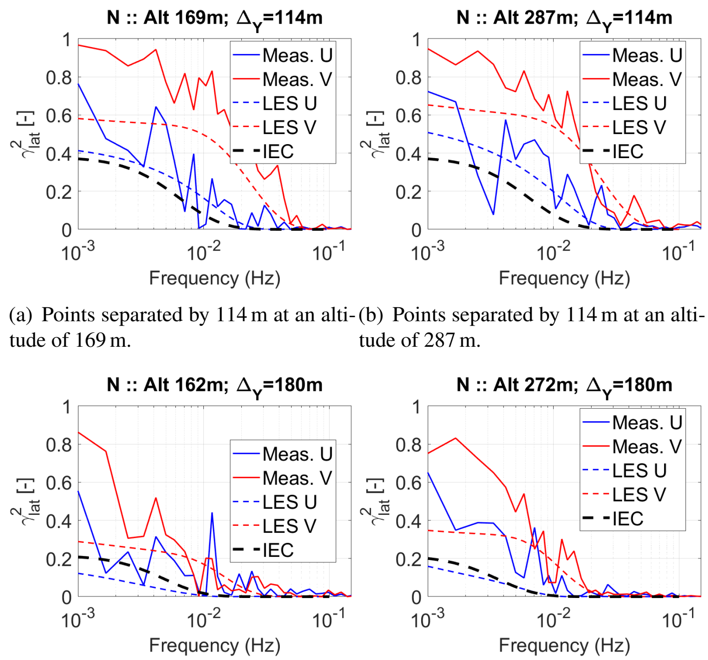

(a) Points separated by 114 m at an altitude of 169 m.

(b) Points separated by 114 m at an altitude of 287 m.

(c) Points separated by 180 m at an altitude of 162 m.

(d) Points separated by 180 m at an altitude of 272 m.

Fig. 1 A comparison of the lateral coherence for the *u* (blue) and *v* (red) components based on measurements (solid lines), LES simulations (dashed lines), and the IEC coherence model (black dashed line) in a NABL.

A first observation that can be made in Figure 1 is that there is an evident difference in $\gamma^2_{uu,\mathrm{lat}}$ and $\gamma^2_{vv,\mathrm{lat}}$ in both the measurements and the LES datasets. This is not captured by the IEC model, thus not allowing for the capture of the flow physics accurately. It may also be noted that the γ^2_{LES} estimates compare well in majority of the frequency range, more so for the u component than for the v component. However, discrepancies exist for the low-frequency regime; this is attributed to the absence of meso-scale forcing in the current LES set-up and the short interval of the data set used for coherence estimates, which was 1000 s thus allowing at most one turnover of an eddy with a frequency of 10^{-3} Hz. This can also be the reason for the poor correspondence at very high altitude of 272 m in Figure 1(d).

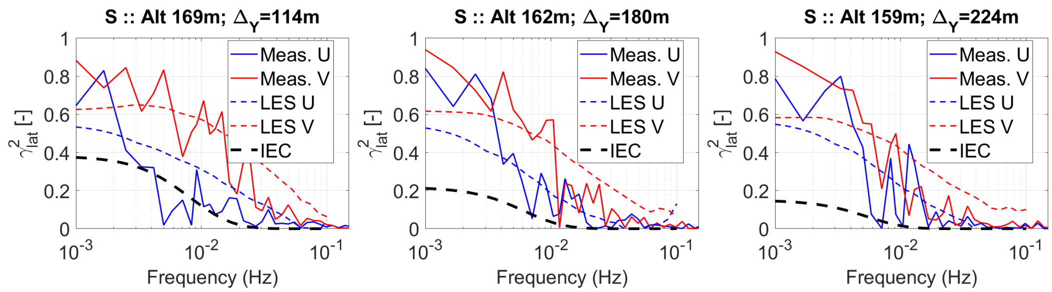

(a) Points separated by 114 m at an altitude of 169 m. (b) Points separated by 180 m at an altitude of 162 m. (c) Points separated by 224 m at an altitude of 159 m.

Fig. 2 A comparison of the lateral coherence for the *u* (blue) and *v* (red) components based on measurements (solid lines), LES simulations (dashed lines), and the IEC coherence model (black dashed line) in a SABL.

Next, in Figure 2, the coherence comparison is provided for the stable ABL. Here, as expected, the correspondence of the IEC coherence to measurements is worse than for the neutral ABL. However, the LES coherence estimates compare well with the measurements through the different altitudes and separations of even up to 224 m, which corresponds to 0.9 D separation for a 20 MW wind turbine of 252 m rotor diameter [10].

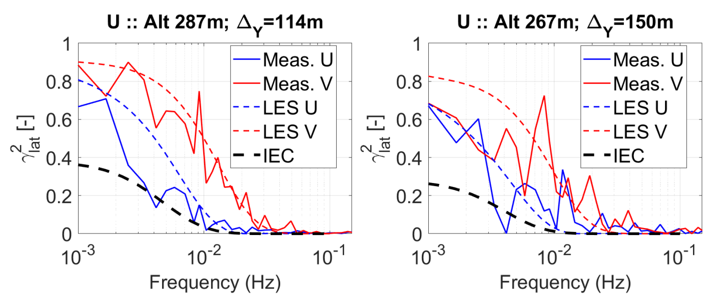

(a) Points separated by 114 m at an altitude of 287 m. (b) Points separated by 150 m at an altitude of 287 m.

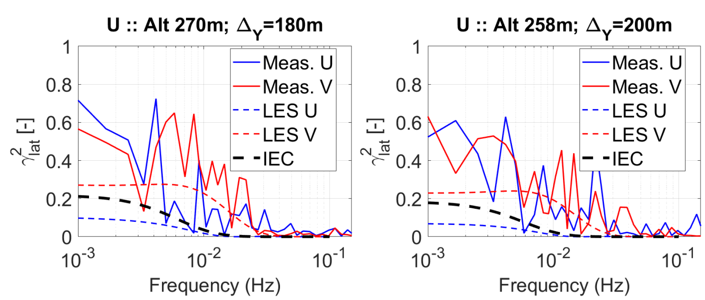

(c) Points separated by 180 m at an altitude of 270 m. (d) Points separated by 200 m at an altitude of 258 m.

Fig. 3 A comparison of the lateral coherence for the *u* (blue) and *v* (red) components based on measurements (solid lines), LES simulations (dashed lines), and the IEC coherence model (black dashed line) in an USABL.

Lastly, the coherence estimates are compared for the unstable ABL in Figure 3. Here, once again, a poor match is seen for the IEC model which is intended for use in a neutral ABL. The LES coherence estimates compare well with the measurements for high altitudes and separations up to 287 m and 250 m, respectively. An underestimation is seen for very large separations in Figure 3(c) and Figure 3(d) at very low frequencies ($\leq$ 0.005 Hz).

V. Evaluation of proposed coherence model against measurements

The proposed coherence model and the methodology to develop it were discussed in subsection III.B and the model was defined by Equation 6. The fitted coherence decay parameter (a_y) and exponent (β_y) obtained after the global optimization are shown in Table 2.

Atmospheric stability	a_y		β_y	
	u component	v component	u component	v component
NABL	35	9	1.16	1
SABL	8	8	0.81	0.88
USABL	39	11	1.36	1.24

Table 2 Proposed lateral coherence model fit parameters for the u and v component.

As intuitively expected, the lateral coherence model decay parameters (a_y) are the smallest for the stable ABL and highest for the unstable ABL. This is attributed to the more frequent horizontal wave-like structures in a stable ABL [40, 41, 30] while vertically stretched eddies in an unstable ABL and diagonally stretched eddies in a neutral ABL [42, 30]. The similar decay exponents (β_y) for the u and v components in the respective ABL, suggest that their coherence decays with frequency (shape of the coherence decay curve) in a comparable manner, reflecting the expected analogous spectral behavior in turbulence across both wind components.

To test the robustness of the model, the resulting coherence estimates are compared against the measurements, rather than with the LES dataset used to tune the model parameters. Similar to section IV, the estimates of $\gamma^2_{uu,\mathrm{lat}}$ and $\gamma^2_{vv,\mathrm{lat}}$ in the measurement samples are compared with the LES counterpart and the IEC model estimate is overlayed. In Figure 4 the $\gamma^2_{uu,\mathrm{lat}}$ is shown for the neutral ABL at various separations and altitudes exactly as in section IV. A notable improvement is seen for the $\gamma^2_{uu,\mathrm{lat,\ model}}$ at lower frequencies in comparison to $\gamma^2_{uu,\mathrm{lat,IEC}}$. Given the neural ABL, for the ≥ 0.005 Hz regime, the proposed model performs similarly to the IEC model estimates for the u component.

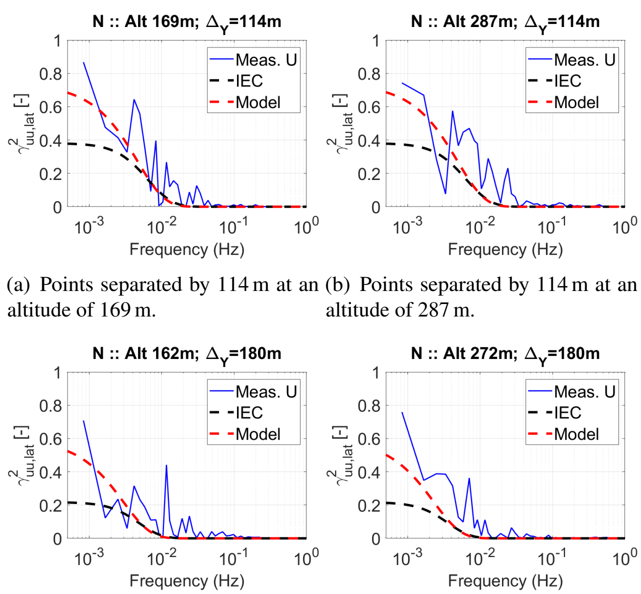

(a) Points separated by 114 m at an altitude of 169 m.

(b) Points separated by 114 m at an altitude of 287 m.

(c) Points separated by 180 m at an altitude of 162 m.

(d) Points separated by 180 m at an altitude of 272 m.

Fig. 4 A comparison of the lateral coherence for the u component based on measurements (solid blue line), the IEC coherence model (black dashed line) and the proposed coherence model (red dashed line) in a NABL.

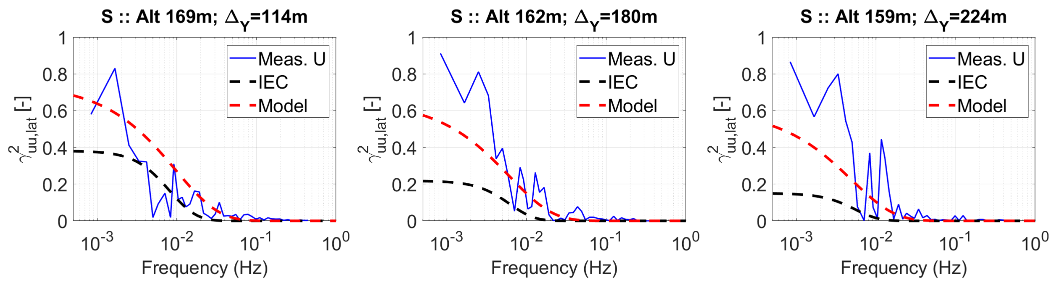

(a) Points separated by 114 m at an altitude of 169 m.
(b) Points separated by 180 m at an altitude of 162 m.
(c) Points separated by 224 m at an altitude of 159 m.

Fig. 5 A comparison of the lateral coherence for the *u* component based on measurements (solid blue line), the IEC coherence model (black dashed line) and the proposed coherence model (red dashed line) in a SABL.

Figure 5 presents the scenario of a stable ABL. Here, it can be seen that $\gamma^2_{uu,\text{lat, LES}}$ corresponds well to the measurements unlike $\gamma^2_{uu,\text{lat, IEC}}$, at all ranges of frequencies. Lastly, the $\gamma^2_{uu,\text{lat, model}}$ is compared to the measurements and $\gamma^2_{uu,\text{lat, IEC}}$ for an unstable ABL in Figure 6. The proposed model once again provides improvement in coherence estimates for the lower frequency regime and it can be observed that for the ≥ 0.01 Hz, the model performs similar to the IEC model estimates for the *u* component.

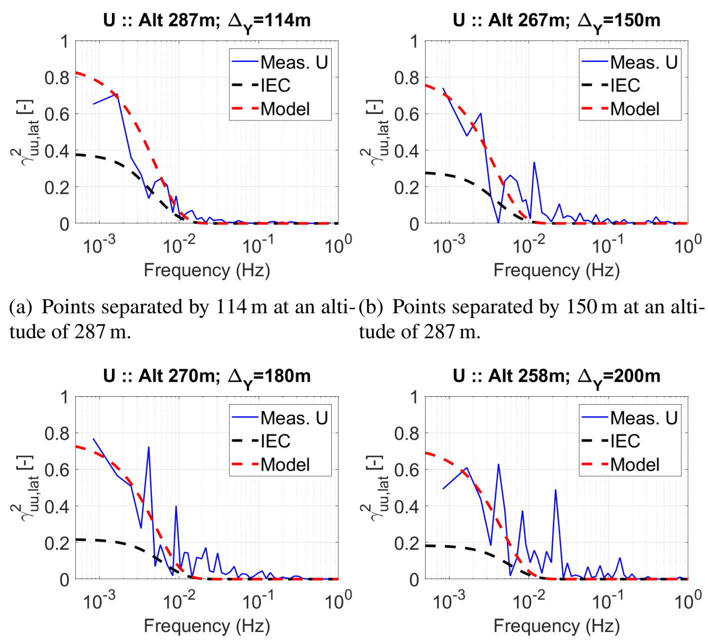

(a) Points separated by 114 m at an altitude of 287 m.
(b) Points separated by 150 m at an altitude of 287 m.
(c) Points separated by 180 m at an altitude of 270 m.
(d) Points separated by 200 m at an altitude of 258 m.

Fig. 6 A comparison of the lateral coherence for the *u* component based on measurements (solid blue line), the IEC coherence model (black dashed line) and the proposed coherence model (red dashed line) in an USABL.

Similar to the above comparison, the estimates of $\gamma^2_{vv,\text{lat, IEC}}$ are provided for the *v* component in a neutral ABL (Figure 7), stable ABL (Figure 8), and an unstable ABL (Figure 9). A remarkable improvement is seen with the $\gamma^2_{vv,\text{lat, model}}$ estimates throughout the different stability regimes, separations and altitudes, in a wide range of frequencies. Upon using the IEC model for the *v* component, it is evident that it leads a significant underestimation in comparison to the measurements and the proposed coherence model. The accurate modelling of the *v* component coherence is important for wake meandering studies but less critical for wind turbine loads [43, 44, 45, 4].

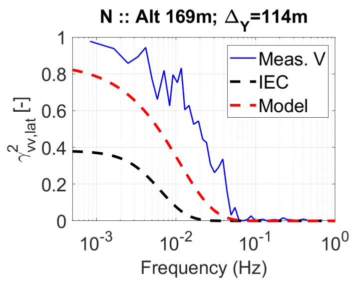

(a) Points separated by 114 m at an altitude of 169 m.

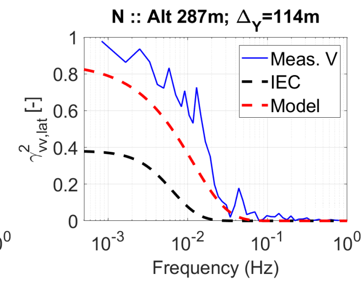

(b) Points separated by 114 m at an altitude of 287 m.

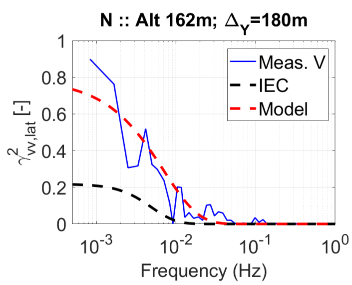

(c) Points separated by 180 m at an altitude of 162 m.

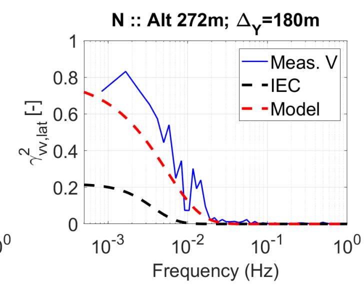

(d) Points separated by 180 m at an altitude of 272 m.

Fig. 7 A comparison of the lateral coherence for the v component based on measurements (solid blue line), the IEC coherence model (black dashed line) and the proposed coherence model (red dashed line) in a NABL.

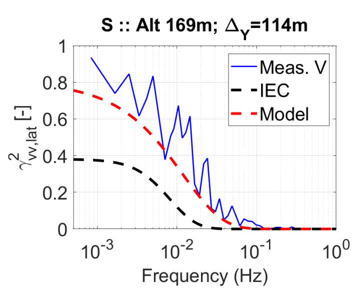

(a) Points separated by 114 m at an altitude of 169 m.

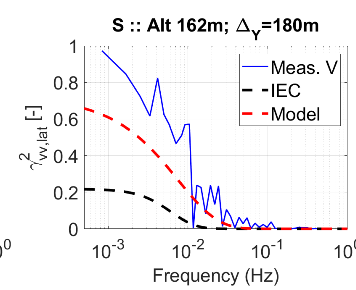

(b) Points separated by 180 m at an altitude of 162 m.

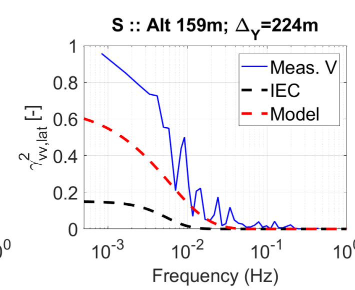

(c) Points separated by 224 m at an altitude of 159 m.

Fig. 8 A comparison of the lateral coherence for the v component based on measurements (solid blue line), the IEC coherence model (black dashed line) and the proposed coherence model (red dashed line) in a SABL.

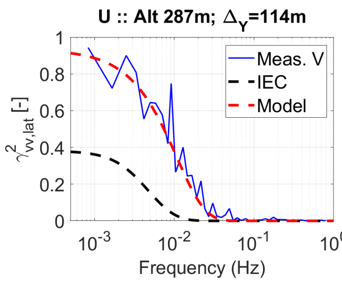

(a) Points separated by 114 m at an altitude of 287 m.

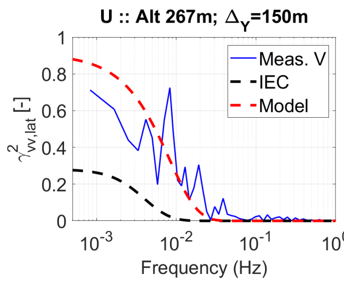

(b) Points separated by 150 m at an altitude of 287 m.

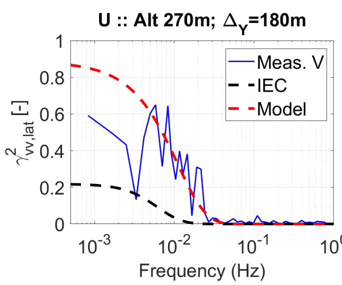

(c) Points separated by 180 m at an altitude of 270 m.

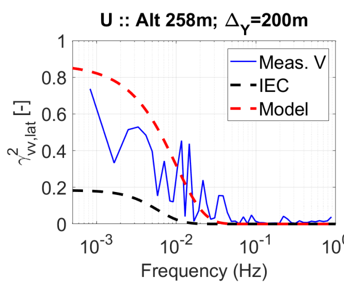

(d) Points separated by 200 m at an altitude of 258 m.

Fig. 9 A comparison of the lateral coherence for the *v* component based on measurements (solid blue line), the IEC coherence model (black dashed line) and the proposed coherence model (red dashed line) in an USABL.

VI. Conclusions

This study focused on modeling the lateral coherence of atmospheric turbulence across a range of atmospheric stability regimes. Large-eddy simulations (LES) were conducted and validated using measurement data from [23], targeting spatial and temporal scales relevant to 20 MW+ wind turbines. The spectral characteristics of the atmospheric boundary layer (ABL) were examined up to altitudes of 300 m, capturing the intricate dynamics of the ABL above the surface layer. A total of nine distinct LES cases were evaluated against measurements, with a specific focus on the coherence of the longitudinal (u) and lateral (v) wind velocity components at altitudes representative of utility-scale wind turbine rotors, and for lateral separations of up to 250 m. Consequently, a new coherence model is proposed (Equation 6) that utilizes a decay parameter and an additional decay exponent, which differ for neutral, stable, and unstable ABLs (Table 2). The model was calibrated on a subset of the LES datasets and then validated with measurements. A noticeable improvement was observed in the match with measurements compared to the current IEC Kaimal coherence model. The current model has a similar computational expense to the IEC Kaimal coherence model and allows for capturing more physics of the ABL. Future work will involve testing the proposed coherence model in aeroelastic simulations and comparing the results with those of the LES counterpart. Future work will also involve expanding the model for vertical coherence capability by accessing a similar measurement campaign at high altitudes, up to 300 m.

Acknowledgments

This research was supported by the Korea Institute of Energy Technology Evaluation and Planning (KETEP) grant, funded by the Korea Government (MOTIE) (20228520020050). The authors thank the Delft High-Performance Computing Centre [46] for the use of computational resources of the DelftBlue supercomputer. The authors thank SURF (www.surf.nl) for the support in using the Dutch National Supercomputer Snellius.

References

[1] Paul Veers et al. "Grand challenges in the design, manufacture, and operation of future wind turbine systems". In: *Wind Energy Science* 8.7 (July 2023), pp. 1071–1131. ISSN: 23667451. DOI: 10.5194/WES-8-1071-2023.

[2] Etienne Cheynet, Jasna B. Jakobsen, and Joachim Reuder. "Velocity Spectra and Coherence Estimates in the Marine Atmospheric Boundary Layer". In: *Boundary-Layer Meteorology* 169.3 (Dec. 2018), pp. 429–460. ISSN: 15731472. DOI: 10.1007/S10546-018-0382-2/TABLES/3. URL: https://link.springer.com/article/10.1007/s10546-018-0382-2.

[3] Alfredo Peña and Sven Erik Gryning. "Charnock's roughness length model and non-dimensional wind profiles over the sea". In: *Boundary-Layer Meteorology* 128.2 (Aug. 2008), pp. 191–203. ISSN: 00068314. DOI: 10.1007/S10546-008-9285-Y/METRICS. URL: https://link.springer.com/article/10.1007/s10546-008-9285-y.

[4] Amy N. Robertson et al. "Sensitivity analysis of the effect of wind characteristics and turbine properties on wind turbine loads". In: *Wind Energy Science* 4.3 (Sept. 2019), pp. 479–513. ISSN: 23667451. DOI: 10.5194/WES-4-479-2019.

[5] Luke D. Nelson et al. "Statistical Analysis of Inflow and Structural Response Data From the LIST Program". In: *ASME 2003 Wind Energy Symposium, WIND2003* (Feb. 2009), pp. 270–282. DOI: 10.1115/WIND2003-867. URL: https://dx.doi.org/10.1115/WIND2003-867.

[6] Korn Saranyasoontorn, Lance Manuel, and Paul S. Veers. "A Comparison of Standard Coherence Models for Inflow Turbulence With Estimates from Field Measurements". In: *Journal of Solar Energy Engineering* 126.4 (Nov. 2004), pp. 1069–1082. ISSN: 0199-6231. DOI: 10.1115/1.1797978. URL: https://dx.doi.org/10.1115/1.1797978.

[7] Jakob Mann, Leif Kristensen, and Michael S Courtney. *The Great Belt coherence experiment. A study of atmospheric turbulence over water*. Risø National Laboratory, 1991. ISBN: 87-550-1747-9. URL: https://orbit.dtu.dk/en/publications/the-great-belt-coherence-experiment-a-study-of-atmospheric-turbul.

[8] Wolfgang Schlez and David Infield. "Horizontal, Two Point Coherence for Separations Greater Than the Measurement Height". In: *Boundary-Layer Meteorology 1998 87:3* 87.3 (1998), pp. 459–480. ISSN: 1573-1472. DOI: 10.1023/A:1000997610233. URL: https://link.springer.com/article/10.1023/A:1000997610233.

[9] Gunner Chr Larsen and Kurt Schaldemose Hansen. *Spatial coherence of the longitudinal turbulence component*. 2003. URL: https://orbit.dtu.dk/en/publications/spatial-coherence-of-the-longitudinal-turbulence-component.

[10] L. Sartori et al. "Preliminary design and optimization of a 20MW reference wind turbine". In: *Journal of Physics: Conference Series* 1037.4 (June 2018), p. 042003. ISSN: 1742-6596. DOI: 10.1088/1742-6596/1037/4/042003. URL: https://iopscience.iop.org/article/10.1088/1742-6596/1037/4/042003.

[11] International Electrotechnical Commission (IEC). *IEC 61400-3-1:2019 | IEC Webstore*. URL: https://webstore.iec.ch/publication/29360.

[12] J. Mann. "The spatial structure of neutral atmospheric surface-layer turbulence". In: *Journal of Fluid Mechanics* 273 (1994), pp. 141–168. ISSN: 0022-1120. URL: https://orbit.dtu.dk/en/publications/the-spatial-structure-of-neutral-atmospheric-surface-layer-turbul.

[13] Jakob Mann. "Wind field simulation". In: *Probabilistic Engineering Mechanics* 13.4 (Oct. 1998), pp. 269–282. ISSN: 0266-8920. DOI: 10.1016/S0266-8920(97)00036-2.

[14] J. C. Kaimal et al. "Spectral characteristics of surface-layer turbulence". In: *Quarterly Journal of the Royal Meteorological Society* 98.417 (July 1972), pp. 563–589. ISSN: 1477-870X. DOI: 10.1002/QJ.49709841707. URL: https://onlinelibrary.wiley.com/doi/full/10.1002/qj.49709841707.

[15] Robert Thresher et al. "Modeling the response of wind turbines to atmospheric turbulence". In: (May 1981).

[16] A G Davenport. "The application of statistical concepts to the wind loading of structures". In: *Proceedings of the Institution of Civil Engineers* 19.4 (1961), pp. 449–472. DOI: 10.1680/iicep.1961.11304. URL: https://doi.org/10.1680/iicep.1961.11304.

[17] R J Barthelmie. "The effects of atmospheric stability on coastal wind climates". In: *Meteorological Applications* 6.1 (1999), pp. 39–47. DOI: https://doi.org/10.1017/S1350482799000961. URL: https://rmets.onlinelibrary.wiley.com/doi/abs/10.1017/S1350482799000961.

[18] Ameya Sathe, Sven-Erik Gryning, and Alfredo Peña. "Comparison of the atmospheric stability and wind profiles at two wind farm sites over a long marine fetch in the North Sea". In: *Wind Energy* 14.6 (2011), pp. 767–780. DOI: https://doi.org/10.1002/we.456. URL: https://onlinelibrary.wiley.com/doi/abs/10.1002/we.456.

[19] A. J. Bowen, R. G.J. Flay, and H. A. Panofsky. "Vertical coherence and phase delay between wind components in strong winds below 20 m". In: *Boundary-Layer Meteorology* 26.4 (Aug. 1983), pp. 313–324. ISSN: 00068314. DOI: 10.1007/BF00119530/METRICS. URL: https://link.springer.com/article/10.1007/BF00119530.

[20] E. Cheynet. "Influence of the Measurement Height on the Vertical Coherence of Natural Wind". In: *Lecture Notes in Civil Engineering* 27 (2019), pp. 207–221. ISSN: 23662565. DOI: 10.1007/978-3-030-12815-9{_}17/FIGURES/6. URL: https://link.springer.com/chapter/10.1007/978-3-030-12815-9_17.

[21] C. Sacré and D. Delaunay. "Structure spatiale de la turbulence au cours de vents forts sur differents sites". In: *Journal of Wind Engineering and Industrial Aerodynamics* 41.1-3 (Oct. 1992), pp. 295–303. ISSN: 0167-6105. DOI: 10.1016/0167-6105(92)90424-9.

[22] Etienne Cheynet et al. "Measurements of Surface-Layer Turbulence in a Wide Norwegian Fjord Using Synchronized Long-Range Doppler Wind Lidars". In: *Remote Sensing 2017, Vol. 9, Page 977* 9.10 (Sept. 2017), p. 977. ISSN: 2072-4292. DOI: 10.3390/RS9100977. URL: https://www.mdpi.com/2072-4292/9/10/977/htm%20https://www.mdpi.com/2072-4292/9/10/977.

[23] Ansh Patel et al. "Trans experiment post-processed data". In: *DTU data repository* (Feb. 2025). DOI: 10.11583/DTU.28390181.v1. URL: https://data.dtu.dk/articles/dataset/Trans_experiment_post-processed_data/28390181.

[24] Matthew Churchfield, Sang Lee, and Patrick Moriarty. "Overview of the Simulator fOr Wind Farm Application (SOWFA)". In: (2012). URL: http://wind.nrel.gov/designcodes/simulators/sowfa/.

[25] H. G. Weller et al. "A tensorial approach to computational continuum mechanics using object-oriented techniques". In: *Computer in Physics* 12.6 (Nov. 1998), pp. 620–631. ISSN: 0894-1866. DOI: 10.1063/1.168744. URL: /aip/cip/article/12/6/620/510187/A-tensorial-approach-to-computational-continuum.

[26] Jason Jonkman, Mike Sprague, and et. al. *OpenFAST | Wind Research | NREL*. 2022. URL: https://www.nrel.gov/wind/nwtc/openfast.html.

[27] Matthew J. Churchfield et al. "A numerical study of the effects of atmospheric and wake turbulence on wind turbine dynamics". In: *Journal of Turbulence* 13 (2012), pp. 1–32. ISSN: 14685248. DOI: 10.1080/14685248.2012.668191. URL: https://www.tandfonline.com/doi/abs/10.1080/14685248.2012.668191.

[28] Chin-Hoh Moeng. "A Large-Eddy-Simulation Model for the Study of Planetary Boundary-Layer Turbulence". In: *Journal of Atmospheric Sciences* 41.13 (1984), pp. 2052–2062. DOI: 10.1175/1520-0469(1984)041<2052:ALESMF>2.0.CO;2. URL: https://journals.ametsoc.org/view/journals/atsc/41/13/1520-0469_1984_041_2052_alesmf_2_0_co_2.xml.

[29] James W Deardorff. "Stratocumulus-capped mixed layers derived from a three-dimensional model". In: *Boundary-Layer Meteorology* 18.4 (1980), pp. 495–527. ISSN: 1573-1472. DOI: 10.1007/BF00119502. URL: https://doi.org/10.1007/BF00119502.

[30] Nirav Dangi et al. "The effect of turbulent coherent structures in atmospheric flow on wind turbine loads". In: *Renewable Energy* 241 (2025), p. 122248. ISSN: 0960-1481. DOI: https://doi.org/10.1016/j.renene.2024.122248. URL: https://www.sciencedirect.com/science/article/pii/S0960148124023164.

[31] P M O Gebraad, M J Churchfield, and P A Fleming. "Incorporating Atmospheric Stability Effects into the FLORIS Engineering Model of Wakes in Wind Farms". In: *Journal of Physics: Conference Series* 753.5 (Sept. 2016), p. 52004. DOI: 10.1088/1742-6596/753/5/052004. URL: https://dx.doi.org/10.1088/1742-6596/753/5/052004.

[32] Srinidhi N. Gadde and Richard J.A.M. Stevens. "Effect of low-level jet height on wind farm performance". In: *Journal of Renewable and Sustainable Energy* 13.1 (Jan. 2021), p. 13305. ISSN: 19417012. DOI: 10.1063/5.0026232/284849. URL: /aip/jrse/article/13/1/013305/284849/Effect-of-low-level-jet-height-on-wind-farm.

[33] Bowen Zhou and Fotini Katopodes Chow. "Turbulence modeling for the stable atmospheric boundary layer and implications for wind energy". In: *Flow, Turbulence and Combustion* 88.1-2 (Mar. 2012), pp. 255–277. ISSN: 13866184. DOI: 10.1007/S10494-011-9359-7/METRICS. URL: https://link.springer.com/article/10.1007/s10494-011-9359-7.

[34] International Electrotechnical Commission (IEC). *IEC 61400-1:2019*. 2019. URL: https://webstore.iec.ch/publication/26423.

[35] Hans A Panofsky and John A Dutton. *Atmospheric turbulence*. 1984.

[36] L. Kristensen and N. O. Jensen. "Lateral coherence in isotropic turbulence and in the natural wind". In: *Boundary-Layer Meteorology* 17.3 (1979), pp. 353–373. ISSN: 15731472. DOI: 10.1007/BF00117924/METRICS. URL: https://link.springer.com/article/10.1007/BF00117924.

[37] Peter D. Welch. "The Use of Fast Fourier Transform for the Estimation of Power Spectra: A Method Based on Time Averaging Over Short, Modified Periodograms". In: *IEEE Transactions on Audio and Electroacoustics* 15.2 (1967), pp. 70–73. ISSN: 00189278. DOI: 10.1109/TAU.1967.1161901.

[38] Eric Simley and Lucy Y. Pao. "A longitudinal spatial coherence model for wind evolution based on large-eddy simulation". In: *Proceedings of the American Control Conference* 2015-July (July 2015), pp. 3708–3714. ISSN: 07431619. DOI: 10.1109/ACC.2015.7171906.

[39] A S Monin and A M Obukhov. "Basic laws of turbulent mixing in the surface layer of the atmosphere". In: *Geophys. Inst. Acad. Sci. USSR* 24.151 (1954), pp. 163–187. URL: https://gibbs.science/efd/handouts/monin_obukhov_1954.pdf.

[40] L. Kristensen et al. “Lateral dispersion of pollutants in a very stable atmosphere—the effect of meandering”. In: *AtmEn* 15.5 (1981), pp. 837–844. ISSN: 1352-2310. DOI: 10.1016/0004-6981(81)90288-2. URL: https://ui.adsabs.harvard.edu/abs/1981AtmEn..15..837K/abstract.

[41] B. M. Koprov et al. “Coherent structures in the atmospheric surface layer under stable and unstable conditions”. In: *Boundary-Layer Meteorology* 111.1 (Apr. 2004), pp. 19–32. ISSN: 00068314. DOI: 10.1023/B:BOUN.0000010996.99753.D3/METRICS. URL: https://link.springer.com/article/10.1023/B:BOUN.0000010996.99753.d3.

[42] Tamino Wetz et al. “Analyses of Spatial Correlation and Coherence in ABL Flow with a Fleet of UAS”. In: *Boundary-Layer Meteorology* 187.3 (June 2023), pp. 673–701. ISSN: 15731472. DOI: 10.1007/S10546-023-00791-4/FIGURES/14. URL: https://link.springer.com/article/10.1007/s10546-023-00791-4.

[43] Kelsey Shaler et al. *FAST.Farm Response to Varying Wind Inflow Techniques: Preprint*. Tech. rep. NREL/CP-5000-72893, Jan. 2019. URL: https://www.nrel.gov/docs/fy19osti/72893.pdf.

[44] A Wise and E E Bachynski. “Analysis of wake effects on global responses for a floating two-turbine case”. In: *Journal of Physics: Conference Series* 1356.1 (Oct. 2019), p. 12004. DOI: 10.1088/1742-6596/1356/1/012004. URL: https://dx.doi.org/10.1088/1742-6596/1356/1/012004.

[45] Adam S Wise and Erin E Bachynski. “Wake meandering effects on floating wind turbines”. In: *Wind Energy* 23.5 (2020), pp. 1266–1285. DOI: https://doi.org/10.1002/we.2485. URL: https://onlinelibrary.wiley.com/doi/abs/10.1002/we.2485.

[46] Delft High Performance Computing Centre (DHPC). “DelftBlue Supercomputer (Phase 2)”. In: (2024). URL: https://www.tudelft.nl/dhpc/ark:/44463/DelftBluePhase2.